Journal of Social Research
P-ISSN: 2827-9832
E-ISSN: 2828-335x
Vol.5, No.3, February 2026
http://ijsr.internationaljournallabs.com/index.php/ijsr

Assessment of Climate Change Vulnerability in the Muara Karang Power Generation Unit

Aulia Rahmanissa*, Joni Hermana
Institut Teknologi Sepuluh Nopember, Indonesia
Email: rahmanissa06@gmail.com*

ABSTRACT

The Muara Karang Generation Unit in North Jakarta is located in a coastal area that is highly vulnerable to climate change, particularly due to rising ambient air temperatures, sea-level rise, and coastal inundation. These impacts have affected the plant's operational performance, including reduced efficiency of gas and steam turbines, increased cooling system loads, and the occurrence of seawater intrusion within the power plant area. Such conditions have the potential to disrupt the reliability of electricity supply to the strategic areas of DKI Jakarta. Therefore, a comprehensive climate vulnerability assessment is required to evaluate the level of risk, as well as the technical and financial implications of climate change on power plant performance. This study employs the Climate Vulnerability Index (CVI) approach, which comprises three components: exposure, sensitivity, and adaptive capacity. Exposure analysis was conducted using historical data on ambient air temperature, sea surface temperature, and sea-level rise for the 1994–2024 period, along with CMIP6 climate projections for 2026–2060 under the SSP1-2.6, SSP2-4.5, and SSP5-8.5 scenarios. Sensitivity was assessed based on reductions in generation capacity due to increased air and seawater temperatures, higher fuel consumption, and the risk of seawater intrusion. Adaptive capacity was evaluated through an assessment of existing climate change adaptation and mitigation measures implemented at the facility. All indicators were normalized and weighted to produce a composite vulnerability index value. The results of the climate vulnerability assessment, based on the parameters of ambient temperature, sea temperature, and sea-level rise at the Muara Karang Power Generation Unit, show index values of 0.36 in 2030 and 0.45 in 2050, corresponding to "low" and "moderate" vulnerability categories, respectively.

Keywords: Muara Karang Power Generation Unit; Climate Vulnerability Index (CVI); Climate Change Impacts

INTRODUCTION

The electricity sector is vulnerable to climate change and extreme weather events that can disrupt the operation of critical infrastructure such as hospitals and water installations (Ashrafi & Parhizkar, 2023). These disruptions can lead to substantial financial losses, making it essential for electricity providers and policymakers to understand their impacts to ensure a reliable electricity supply (Stanton et al., 2016).

Several electricity infrastructures are located in North Jakarta, one of which is the Muara Karang Generation Unit in Penjaringan District. The Muara Karang Generation Unit serves the VVIP area of DKI Jakarta, including the State Palace Complex, MPR/DPR Building, government offices, MRT public transportation system, and Soekarno-Hatta International Airport. This strategic role requires the Muara Karang plant to maintain high readiness and reliability in electricity supply operations. Adverse weather events affecting this facility include flooding caused by heavy rainfall and reduced turbine efficiency resulting from rising ambient temperatures (Handayani et al., 2019).

The Muara Karang Generation Unit is located in a coastal area of North Jakarta that is highly vulnerable to the impacts of climate change. In 2021, several instances of waterlogging were observed—likely caused by seawater intrusion—particularly near the outfall and water intake areas. With an elevation of about 0–2 meters above sea level, North Jakarta is highly affected by both land subsidence and sea-level rise (Utara, 2024) (Varrani &

Nones, 2018). Research by (Firman et al., 2011) reported that approximately 40% of Jakarta lies below sea level, with the majority of these low-lying areas concentrated in North Jakarta. This condition increases both the extent of inundation and the strength of tidal currents (Surya et al., 2019). According to Takagi et al. (2016), flood projections for the coastal area of Jakarta from 2000 to 2050 indicate an expansion of inundated areas up to 110.5 km², driven largely by land subsidence.

Several studies on climate change vulnerability in the electricity sector have been conducted to evaluate system readiness and response capacity (Burillo et al., 2019; Craig et al., 2018; Mukherjee & Nateghi, 2017; Panteli et al., 2017; Panteli & Mancarella, 2015). Climate change and variations in water resources can directly affect electricity generation capacity amid growing energy demand (Van Vliet et al., 2016). This study specifically addresses climate vulnerability in this context.

The urgency of addressing this gap cannot be overstated. Decisions on major infrastructure upgrades—such as turbine overhauls or the construction of protective seawalls—entail multi-million-dollar investments with long operational lifespans. These decisions must be guided not only by historical climate data but also by robust projections of future climatic conditions over the asset's lifetime. As emphasized by the IPCC (2022), the window for proactive adaptation is rapidly closing. For a facility as strategically vital as Muara Karang, understanding its future vulnerability is not merely an academic exercise but a national imperative to ensure the continuity of essential government and public services.

The novelty of this research lies in its integrated, multi-method approach. To the best of the authors' knowledge, it is the first comprehensive climate vulnerability assessment conducted for an Indonesian power plant. The study: (1) applies the latest CMIP6 climate projections under multiple SSP scenarios for the key impact variables—ambient air temperature, sea surface temperature, and sea-level rise; (2) calibrates these projections with extensive historical in-situ operational data from the plant, including performance test records and water intake monitoring data, to improve local accuracy; (3) quantifies the plant's sensitivity by deriving power loss functions directly from turbine performance curves; (4) performs an on-site evaluation of existing adaptive capacity; and (5) integrates all these elements into a single, quantitative Climate Vulnerability Index (CVI) for two future time horizons—2030 and 2050. This framework provides a holistic and empirically grounded risk profile for the plant under changing climate conditions.

The primary objective of this research is to assess the vulnerability of the Muara Karang Power Generation Unit to climate change by the years 2030 and 2050. This overarching goal is structured into several key objectives: (1) to analyze historical trends (1994–2024) and future projections (2026–2060) of ambient air temperature, sea surface temperature, and sea-level rise near the plant; (2) to quantify operational sensitivity, particularly power output losses in gas and steam turbines due to temperature increases and inundation risks; (3) to evaluate existing adaptive capacities, both structural (e.g., embankments, pumps) and non-structural (e.g., SOPs, emergency response systems); and (4) to integrate all components into a composite Climate Vulnerability Index to categorize overall risk levels.

This research is expected to provide significant theoretical and practical contributions. Theoretically, it advances the field of climate risk assessment for critical infrastructure by

showcasing a replicable method for applying the CVI framework at the asset level, integrating top-down climate projections with bottom-up operational data. Practically, the study delivers actionable insights for PLN (the State Electricity Company) and other key stakeholders. The quantified vulnerability scores and identification of key risk drivers will support targeted, evidence-based adaptation planning. This could involve prioritizing investments in turbine inlet cooling technologies, enhancing cooling water pump capacity, increasing the height of protective embankments, or reinforcing critical equipment against inundation. Ultimately, this research aims to strengthen the long-term operational resilience of the Muara Karang plant, thereby safeguarding the electricity supply for Jakarta's most essential public and government functions in a changing climate.

METHOD

This stage includes a literature study to get an overview of the research to be carried out as well as a review of the supporting literature. The literature study includes geographical conditions in the research area, namely North Jakarta, studies on climate vulnerability studies that have been carried out in coastal areas, studies related to the influence of climate change on the electricity system, especially power generation units.

The location of this study is the Muara Karang Generation Unit which is located in Penjaringan District, North Jakarta and can be seen in the following image. Geographically, the location of the unit is in the coastal area of North Jakarta which is affected by sea level rise, increasing the potential for inundation and strengthening tidal currents.

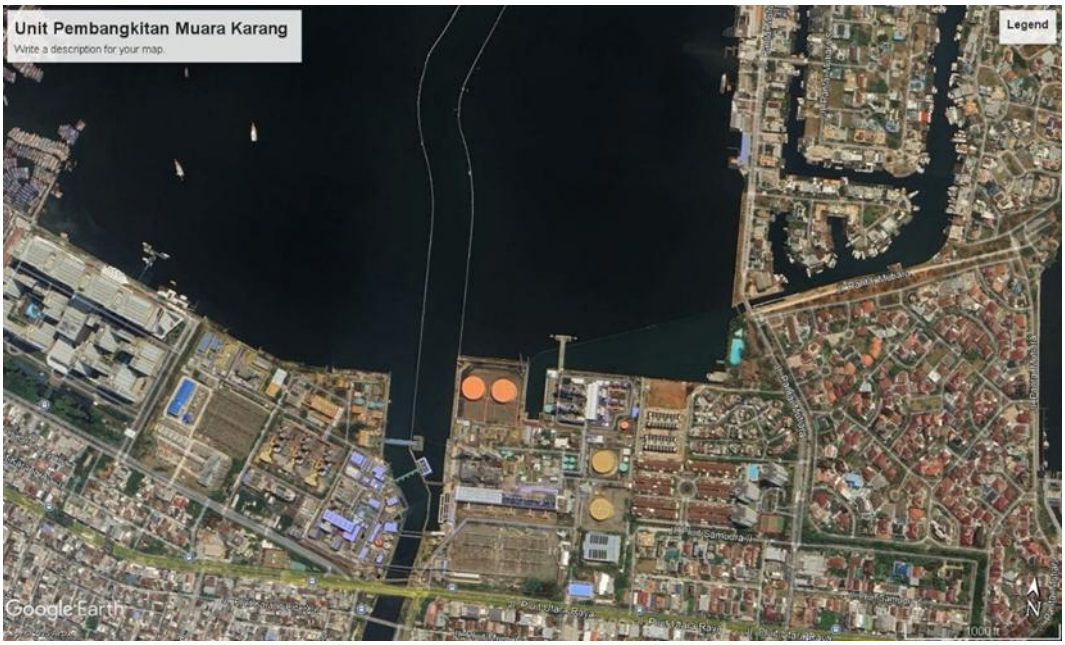

Figure 2. 1 Research Location

The analysis carried out includes:

a. Exposure Analysis

This section is an analysis of indicators related to *exposure*, namely air temperature, seawater temperature, and sea level rise. The data was analyzed for historical trends from

1994-2024. Furthermore, the trend data is compared with the temperature data owned by the generating unit and (in situ data). The in situ temperature data was obtained from monthly performance test data and seawater temperature monitoring data from water intake owned by the company in 2010-2024. Validation using *Root Mean Square Error* (RMSE) measures the average error between the model value and the observation value and Pearson r to assess the pattern fit and liner relationships of the dataset.

- Root Mean Square Error (RMSE):

$$RMSE = \sqrt{\frac{1}{n}\sum_{i=1}^{n}\left(T_{unit,i} - T_{ERA5,i}\right)^2} \quad (2.1)$$

Where,

$T_{unit,i}$ = temperature from units of year i
$T_{ERA5,I}$ = temperature from ERA5 data year i
n = amount of data

- Pearson r:

$$r = \frac{\sum\left(T_{unit,i} - \overline{T}_{unit}\right)\left(T_{ERA5,i} - \overline{T}_{ERA5}\right)}{\sqrt{\sum\left(T_{unit,i} - \overline{T}_{unit}\right)^2 \sum\left(T_{ERA5,i} - \overline{T}_{ERA5}\right)^2}} \quad (2.2)$$

Where,

r = value of correlation coefficient
$T_{unit,i}$ = temperature from units of year i
$\overline{T}_{unit}$ = average unit data temperature
$T_{ERA5,i}$ = temperature from ERA5 data year i
$\overline{T}_{ERA5,i}$ = average temperature of ERA5 data

Once validated, the temperature data is then projected with one of three selected SSP scenarios, namely SSP1-2.6, SSP 2-4.5, or SSP 5-8.5. The projection data set uses *the The Coupled Model Intercomparison Project Phase 6* (CMIP6) dataset for 2026-2060. Before projections, all climate data is corrected. The purpose of correcting historical data and projection data from CMIP6 needs to be done to reduce bias. In this study, the correction calculation uses the delta method, which is calculated from the difference between the average projection data and historical data. The formula used to correct the temperature data is as follows:

- Calculating the Temperature Delta (ΔT) of CMIP6 in the year y

$$\Delta T_{CMIP6(y)} = T_{future,CMIP6,y} - \overline{T}_{historis,CMIP6} \quad (2.3)$$

Where:

$\overline{T}_{historis,CMIP6}$ = average temperature in CMIP6 historic
$T_{future,CMIP6,y}$ = projected temperature of CMIP6 years y

- Projections Per Year (Time-Series)
  To produce a projected temperature series that has been corrected annually

$$T_{corrected\ (y)} = \Delta T_{CMIP6(y)} + \overline{T}_{baseline} \quad (2.4)$$

Where:

$T_{corrected(y)}$ = Corrected projection temperature in year y
$\Delta T_{CMIP6(y)}$ = delta temperature in year y
$\bar{T}_{baseline,unit}$ = average baseline data (in situ data from units)

Sea level rise data analyzed from *sea level anomaly* (SLA) obtained from the formula used to correct the surface rise data a is as follows:

- Average historical data from 1995-2014 to equate with IPCC data

$$SLA_{hist,baseline} = mean\ (SLA_{1995-2014}) \quad (2.5)$$

- Absolute sea level relative, to align to historical baseline

$$ASL_{baseline} = SLA_{baseline} + SLR_{IPCC} \quad (2.6)$$

- Increase or difference (Δ) from the actual condition or the last historical data

$$\Delta \text{from last} = ASL_{baseline} + SLA_{last} \quad (2.7)$$

The projection results from the selected scenario were used for the next sensitivity analysis. Each of these data indicators is normalized with the Min-Max formula with a range of 0-1.

$$X' = \frac{X - X_{min}}{X_{max} - X_{min}} \quad (2.8)$$

Where,

X' = normalized values
X = data in selected year
Xmin = smallest value of the data range
Xmax = highest value of the data range

All indicators that have been normalized, are then used to calculate the exposure value using the following formula:
The total value of the exposure indicator is calculated using the formula:

$$E = \sum_{i=1}^{n} (W_i \times X_i) \quad (2.9)$$

Where,

E = Total exposure value
W_i = Weights for each indicator
X_i = Normalized indicator value (0-1)
n = Number of indicators that make up exposure

b. Sensitivity Analysis

Sensitivity analysis includes the influence of ambient air on turbine gas performance, the effect of seawater temperature on steam turbine performance, and the effect of sea level rise on the area of seawater intrusion. The ambient air temperature sensitivity value and sea surface temperature are calculated from the loss of power by using Equation 2.10.

$$Power\ Loss\ \left(\frac{MW}{^{\circ}C}\right) = Output\ ratio\ \times Capacity\ Nett \qquad (2.10)$$

This sensitivity is seen from incident data related to seawater intrusion obtained from civil monitoring data of power generation units. The next step is to collect the digital elevation model (DEM) data used in this study from the Copernicus GLO-30 dataset developed by the Copernicus Programme with a spatial resolution of about 30 meters, so that it is able to adequately represent the topography of the coastal lowlands. Sea Level Rise (SLR) projection data were obtained from the IPCC AR6 projection raster based on the output of the CMIP6 climate model for various emission scenarios (SSP1-2.6, SSP2-4.5, and SSP5-8.5), which represent the change in average sea level relative to the 1995–2014 global baseline. The SLR projection raster for each SSP scenario was then overlaid with the Copernicus GLO-30 DEM using *a geospatial overlay* approach using Google Earth Pro, after first being converted to a georeferenced visual format (KMZ). This overlay allows for spatial alignment between future sea level projections and existing land topographic conditions.

c. Adaptive Capacity Analysis

The unit's environmental management data and assessment results related to seawater intrusion are used to analyze the adaptations that have been carried out today to deal with climate change. The data is given a score and weighting to obtain the final value of adaptive capacity. The final value of adaptive capacity is further normalized by the following calculations:

$$AC_{norm} = \frac{Adaptive\ Capacity\ Score}{Maximum\ score} \qquad (2.11)$$

Where,

AC_{norm} = normalized adaptive capacity value
Adaptive capacity score = score based on assessment
Maximum score = maximum score of adaptive capacity assessment

d. Vulnerability Calculation

Composite indices are used to quantify the vulnerability, risk, or resilience of multiple indicators into a single synthetic score that can be mapped and compared across regions. This approach is commonly used for multi-hazard disaster vulnerability (Beccari, 2016). In the condition that all values have been normalized, it can use linear aggregation (additives) and then classify them into vulnerability classes. Vulnerability will be measured through 3 points, namely, Exposure, Sensitivity, and Adaptive Capacity with the following formula:

$$VI = \frac{E + S + (1 - AC)}{3} \qquad (2.12)$$

Where,

VI = Vulnerability score
E = Exposure score
S = Sensitivity score
AC = Adaptive capacity score

RESULTS AND DISCUSSION

3.1 Historical trend

In conducting the vulnerability assessment, the selected variables—namely ambient air temperature, sea surface temperature, and sea level rise—were analyzed based on both historical trends and future projections. Historical trend data for air temperature and sea surface temperature were obtained from the ERA5 Reanalysis (Single Levels) dataset provided by the Copernicus Climate Data Store (CDS). Sea level rise was assessed using Sea Level Anomaly (SLA) data, which represent deviations of current sea level relative to the long-term climatological mean over multiple decades. SLA data capture the combined effects of thermal expansion of seawater, land ice melt, and changes in ocean mass, which constitute the primary drivers of sea level rise (Jia et al., 2022). The historical datasets analyzed cover the period 1994–2024 for air temperature and sea surface temperature, and 1993–2023 for sea level anomaly data.

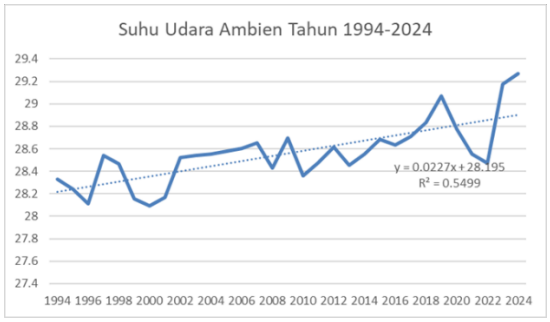

Figure 3. 1 Annual Air Temperature Trends

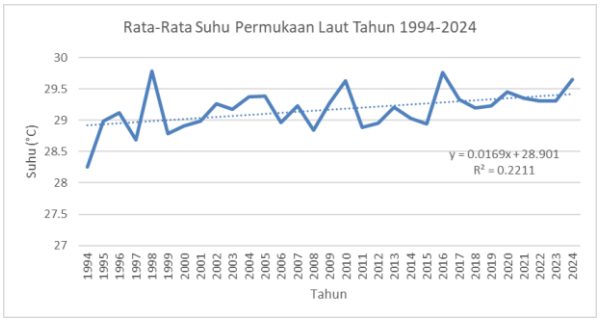

Figure 3. 2 Annual Sea Surface Temperature (SST) Trends

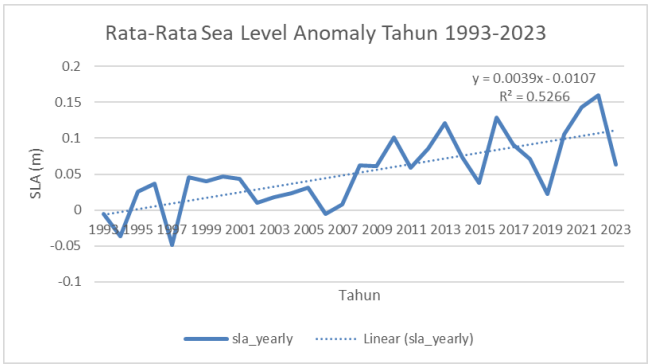

Figure 3. 3 Annual Sea Level Anomaly (SLA) Trends

Sea surface temperature during the observation period ranged between 28.5 °C and 29.6 °C, with the lowest temperatures recorded at the beginning of the period (approximately

1994–1996) and the highest toward the end of the period (around 2024). Although the increase exhibits interannual fluctuations, the long-term warming trend is evident. The rise in sea surface temperature in tropical regions, including Jakarta Bay and the Java Sea, forms part of the broader regional warming phenomenon in the western Indo-Pacific waters, commonly referred to as the Indo-Pacific Warm Pool. According to Roxy et al. (2020), this region has experienced an average sea surface temperature increase of approximately 0.15–0.20 °C per decade over the past 50 years, contributing to shifts in precipitation patterns and an increased intensity of extreme events across Southeast Asia.

Subsequently, ambient air temperature and sea surface temperature were validated against in situ data from the power generation unit. Ambient air temperature data were obtained from recorded measurements in the unit's performance reports, while in situ seawater temperature data were derived from routine monitoring at the intake point. Satellite-based and reanalysis air temperature datasets often differ from ground-based measurements due to differences in spatial resolution, temporal sampling, and the surface characteristics represented (Martin et al., 2019). In situ data (direct field measurements) provide high accuracy at the specific measurement location; however, their spatial coverage is highly limited and may not adequately represent temperature variability within a single satellite or reanalysis grid cell, which typically covers a much larger area. herefore, evaluation and validation of satellite and reanalysis data against in situ observations are essential to quantify bias magnitude and to understand the characteristics of any discrepancies, particularly in regions with high spatial heterogeneity (Pan et al., 2024).

Further validation was conducted using the Root Mean Square Error (RMSE) to quantify the average difference (error) between unit-measured temperatures and ERA5 data in °C (Equation 2.1), while the interannual pattern agreement was assessed using the Pearson correlation coefficient (r) as presented in Equation 2.2. The RMSE for ambient air temperature between ERA5 and in situ data was 2.81°C, with a Pearson correlation coefficient of 0.5. These results indicate that both datasets exhibit a consistent interannual variability pattern and a similar trend direction, as reflected by the moderate positive correlation ($r = 0.5$). The correlation was calculated based on annual mean temperature data, thereby representing similarity in year-to-year fluctuations rather than seasonal or daily variability. This finding supports the use of ERA5 as the historical climate baseline and the unit's in situ data as the operational baseline for climate impact analysis.

The RMSE for sea surface temperature between ERA5 data and in situ measurements was 1.64°C, with a Pearson correlation coefficient of 0.02. This result indicates that temperature variability at the intake point is not primarily governed by offshore SST conditions but is instead strongly influenced by local factors such as mixing processes, water depth, coastal currents, tidal dynamics, and thermal discharge effects from the power plant. Therefore, the in situ data were not used to validate ERA5 or CMIP6 as representations of regional climate conditions; rather, they were treated as indicators of localized operational conditions relevant to turbine performance analysis.

3.2 Projection for 2026-2060

The projection dataset used in this study was derived from The Coupled Model Intercomparison Project Phase 6 (CMIP6), the latest generation of global climate models and projections developed by research centers worldwide. CMIP6 serves as the primary scientific

basis for climate change analysis in the IPCC Sixth Assessment Report (AR6) and is officially distributed through the Copernicus Climate Data Store (CDS).

In this study, SSP2-4.5 was selected as the primary projection scenario, representing a moderate mitigation pathway, although SSP5-8.5 exhibits the most significant and consistent temperature increase throughout the 2026–2060 period. SSP2-4.5 is designed to reflect a world of moderate economic growth and population, as well as mitigation policies that are neither too ambitious nor weak (Bompard et al., 2023; Carleton & Hsiang, 2016; Zhou et al., 2019). Recent literature and the IPCC AR6 indicate that SSP5-8.5 is now considered "very unlikely" given current energy trends and future projections, which are more aligned with intermediate scenarios such as SSP2-4.5. Despite its lower probability, SSP5-8.5 remains useful for stress-testing system resilience and assessing upper-bound risks; however, it should not be interpreted as the most probable future pathway (Scafetta, 2023). Based on these considerations, SSP2-4.5 was adopted as the main scenario for air temperature projection calculations in this study, while SSP5-8.5 was included as a worst-case scenario for comparative analysis.

To estimate projections of ambient air temperature and sea surface temperature, bias correction was first applied using Equation 2.3, followed by time-series projection calculations using Equation 2.4. The correction method used is the *delta method* (delta change). CMIP6 is calculated using the difference between the average of future projections and the average of historical periods (1995–2014). The temperature change delta is then added to the observation baseline to produce a bias-corrected temperature projection. This method is known as the *Additive Delta Method*, and is used by the IPCC AR6, Copernicus C3S, and the World Bank CCKP. The delta method showed slightly better performance in reducing bias in global climate models compared to GAMs and *quantile mapping*. However, the three methods still show considerable variation in performance spatially and temporally (Beyer, et.al, 2020).

The resulting projection outputs are presented in the following figure.

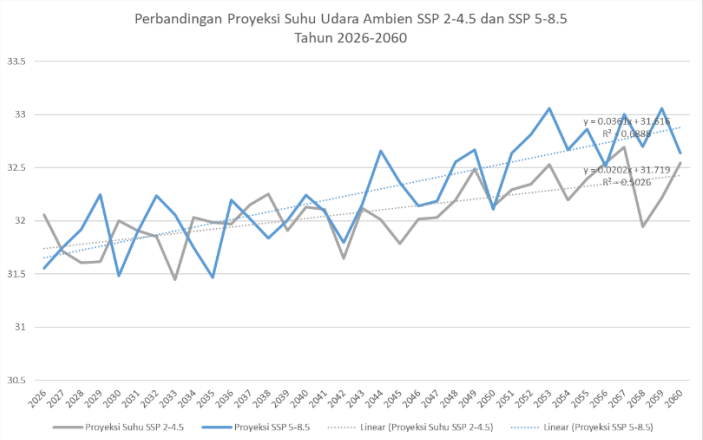

Figure 3. 4 Corrected Ambient Temperature Projection

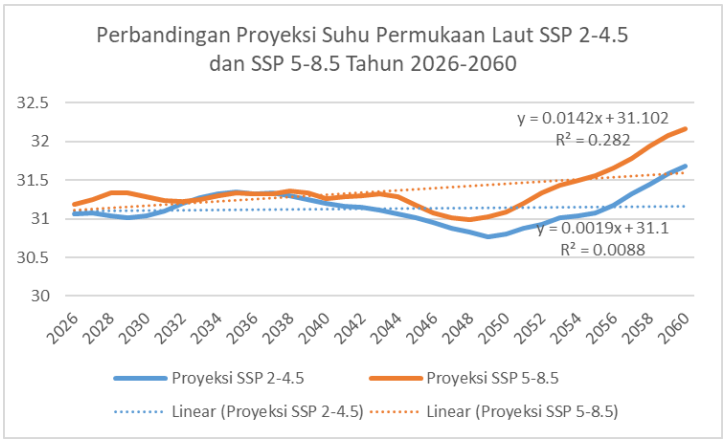

Figure 3. 5 Corrected Sea Surface Temperature Projection

The projected ambient air temperature for the power generation unit over the 2026–2060 period indicates that both SSP2-4.5 and SSP5-8.5 scenarios exhibit a consistent upward warming trend over time. However, the rate and magnitude of projected temperature increases differ between the scenarios. SSP5-8.5 shows a more pronounced warming rate compared to SSP2-4.5, as reflected by a steeper trend line and higher maximum temperature values, particularly after 2040. This difference highlights the influence of higher greenhouse gas emission pathways under SSP5-8.5 on local thermal conditions.

In addition, the projected sea surface temperature ranges between 30.8°C and 31.7°C. Studies of SST in Southeast Asian waters project increases of up to 4.2°C in the Gulf of Thailand and the Malacca Strait by the end of the century, superimposed on an already warm tropical baseline (Salehie et al., 2020). Furthermore, CMIP6-based studies for the Asian Marginal Seas, including Indonesian waters, project warming of approximately 1.7–3.4°C per century under the SSP2-4.5 scenario, with a pronounced summer warming bias in Indonesian waters (Jin, 2023). Therefore, the projected SST range of 30.8–31.7°C in this study remains consistent with both observational trends and CMIP6 regional projections.

For sea level rise projections, the study utilized IPCC AR6 sea level rise data for the years 2030 and 2050, which were accessed through Google Earth Engine. Prior to projection analysis, bias correction was performed by integrating the historical trend (SLA data) with the IPCC SLR projections to avoid abrupt discontinuities. This adjustment was necessary because the two datasets are referenced to different baselines and therefore required alignment. The bias correction was conducted using the delta method, following Equations 2.5 and 2.6, and subsequently refined using Equation 2.7. The results of the 2030 and 2050 sea level rise projections are presented in the table below.

Table 3. 1 Calculation of Sea Level Rise Correction in 2030 and 2050

Year	Scenario	IPCC mean SLR (m)	Baseline mean (m)	Last SLA (m)	ASL_baseline (m)	Projected SLA (m)	Δ from last (m)	Δ from last (mm)
2030	SSP126	00834	0.0418	−0.0060	0.1253	0.0774	0.1313	131.3
	SSP245	0.0831	0.0418	−0.0060	0.1249	0.0771	0.1309	130.9
	SSP585	0.0901	0.0418	−0.0060	0.1319	0.0841	0.1379	137.9

2050	SSP126	0.18	0.0418	−0.0060	0.2218	0.174	0.2278	227.8
	SSP245	0.192	0.0418	−0.0060	0.2338	0.186	0.2398	239.8
	SSP585	0.221	0.0418	−0.0060	0.2628	0.215	0.2688	268.8

The bias-corrected results indicate that Jakarta Bay is projected to experience a substantial increase in sea level over the coming decades. By 2030, all IPCC scenarios (SSP1-2.6, SSP2-4.5, and SSP5-8.5) produce relatively similar sea level rise estimates, ranging from 130.9 to 137.9 mm relative to the most recent observational baseline in 2023. This convergence is consistent with IPCC AR6 findings, which emphasize that in the near term, differences among emission scenarios remain limited because the ocean system responds gradually to warming, primarily through thermal expansion and ice melt processes that require decades to manifest significantly. Consequently, projected sea level rise up to 2030 shows minimal divergence across SSP scenarios, as internal climate variability plays a more dominant role than emission pathway differences during this period. Scenario divergence becomes more pronounced after 2050, driven by cumulative emissions and delayed climate system responses (Sung et al., 2021).

3.3 Exposure Analysis

Based on physical relevance, the degree of influence on system efficiency, and observed trend results, weighting of the indicators was applied. Vulnerability assessments using composite indices almost invariably require weighting. An evidence-based weighting approach was adopted to enhance transparency and validity by deriving weights from empirical findings. The weighting values for each indicator were obtained through a literature review. The selected studies were evaluated according to the magnitude and immediacy of the impacts associated with each exposure indicator, such that indicators producing faster and more directly observable effects were assigned higher weights.

Table 3. 2 Determination of Exposure Sub-Indicator Weights

No	Sub-Indicator Exposure	Description of Impact on the Power Plant	Weighting (%)
1	Increase in Ambient Air Temperature	Directly affects gas turbine thermal efficiency and power output.	35
2	Sea Surface Temperature	Reduces condenser cooling system effectiveness and increases the risk of thermal stress.	35
3	Sea Level Rise	Increases the risk of flooding, coastal erosion, and disruptions to the cooling water system in coastal areas.	30
		TOTAL	**100%**

The result of exposure calculation as follows:

Table 3. 3 Exposure Calculation

Indicator	$E_{i,2030}$	$E_{i,2050}$	Weight	E total 2030	E total 2050
Ambient temperature	0,443	0,553	0,35	0,155	0,193
Sea surface temperature	0,300	0,046	0,35	0,105	0,016
Sea level rise	0,546	1,000	0,3	0,164	0,3
				0,424	0,510
				Moderate	Moderate

To evaluate the robustness of the exposure weights against uncertainty and residual subjectivity in indicator weighting, a sensitivity test was conducted by varying each indicator's weight by ±5% and ±10% from its baseline value, while maintaining a total weight of 100%. The results indicate that these weight variations produced only marginal changes in the Exposure values and did not lead to any shift in exposure category. Therefore, the baseline weighting structure is considered sufficiently robust and representative.

The Exposure value for each scenario was calculated using Equation 2.9, with indicator values previously normalized according to Equation 2.8. The assessment was conducted for the projection years 2030 and 2050. The resulting Exposure values were subsequently classified according to the exposure categories presented in the table below.

Table 3. 4 Exposure Value Classification

Exposure Value Range	Category
0 - 0,20	Very low
0,2 – 0,4	Low
0,4 - 0,6	Moderate
0,6 – 0,8	High
0,8 – 1	Very high

3.4 Sensitivity Analysis

Sensitivity indicators are used to determine the extent to which a system is affected by climate change or climate variability. In this study, sensitivity is assessed in relation to ambient air temperature, sea surface temperature, and sea level rise. The sensitivity analysis examines how changes in operational efficiency and infrastructure conditions influence the exposure value, which represents the degree to which the power plant is subjected to climate change impacts.

3.4.1 Sensitivity to Ambient Temperature

Previous studies indicate that increasing ambient air temperature has a significant negative impact on the performance of combined cycle power plants, primarily by reducing power output and overall efficiency. Higher ambient temperatures decrease air density, resulting in a lower mass flow rate of air entering the gas turbine. The reduced oxygen availability directly leads to a decline in the power output of both the gas turbine and the

steam turbine (Aslan & Büyükköse, 2025). In this analysis, the assessment was conducted based on three gas turbines operating in Block 1, Block 2, and Block 3.

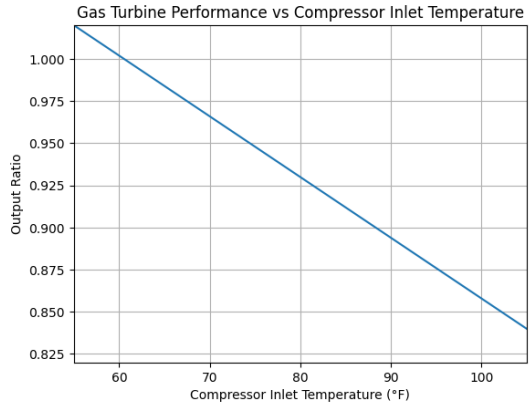

Figure 3. 6 Gas Turbine Performance Graph of Block 1 with Respect to Inlet Temperature

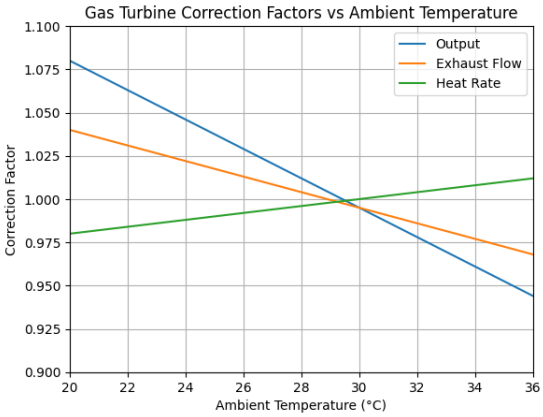

Figure 3. 7 Gas Turbine Performance Graph of Block 2 with Respect to Inlet Temperature

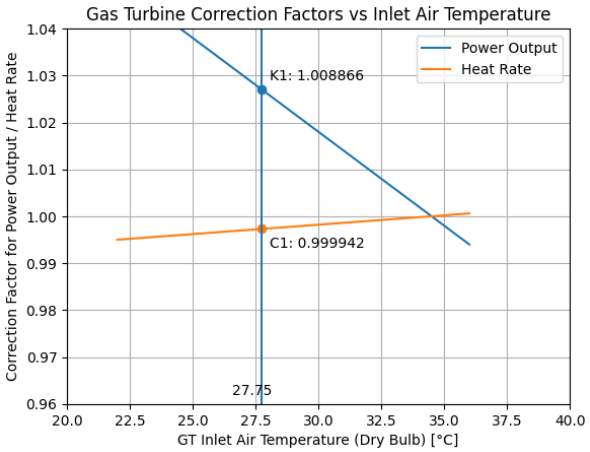

Figure 3. 8 Power Output Correction Block 3

From each of the performance graphs above, the reduction in output ratio can be determined and subsequently used to calculate the total power loss of the gas turbine. The graphs illustrate the correlation between gas turbine performance and ambient air temperature, enabling the determination of correction factors under specific temperature conditions. These correction factors are then multiplied by the gas turbine capacity to estimate the resulting power output. The calculated output ratio reduction and corresponding power loss are presented in the table below.

Table 3. 5 Power Loss Calculation per 1°C Increase

Block	Unit	Capacity Nett (MW)	Output Ratio Decrease	Power Loss (MW/°C)
Block 1	GT 1.1	90	-0,0064	0,675
	GT 1.2	90	-0,0064	0,675
	GT 1.3	100	-0,0064	0,675
Block 2	GT 2.1	250	-0,0062	0,1557

	GT 2.2	250	-0,0062	0,1557
Block 3	GT 3.1	330	-0,004	2
TOTAL		**1080**		**6,047**

The calculation indicates that the total power loss amounts to 1.080 MW, resulting in an overall plant sensitivity of 0.0056, or 0.56%. This value implies that each 1°C increase in ambient temperature leads to a 0.56% reduction in the plant's total available capacity. The cumulative effect of such power reductions may significantly impact annual energy production, particularly under future climate conditions projected to experience continued temperature increases.

3.4.2 Sensitivity to Sea Surface Temperature

Seawater is utilized as cooling water to regulate equipment temperature. Power plants employing recirculating cooling systems are generally more sensitive to temperature increases compared to once-through systems. Gas-fired power plants also tend to be more sensitive to temperature changes than coal-fired plants (Petrakopoulou et al., 2020). Literature indicates that rising seawater temperature, when used as a cooling medium, reduces condenser efficiency, increases condenser pressure, and decreases steam turbine output by approximately 0.17% or about 1.8 MW per 1°C increase, depending on the plant type and capacity (Aslan & Büyükköse, 2025).

In this report, the performance curve of the steam turbine (Block 2 Combined Cycle Unit) in relation to seawater temperature at the condenser inlet has been obtained. The corresponding graph is presented in the figure below.

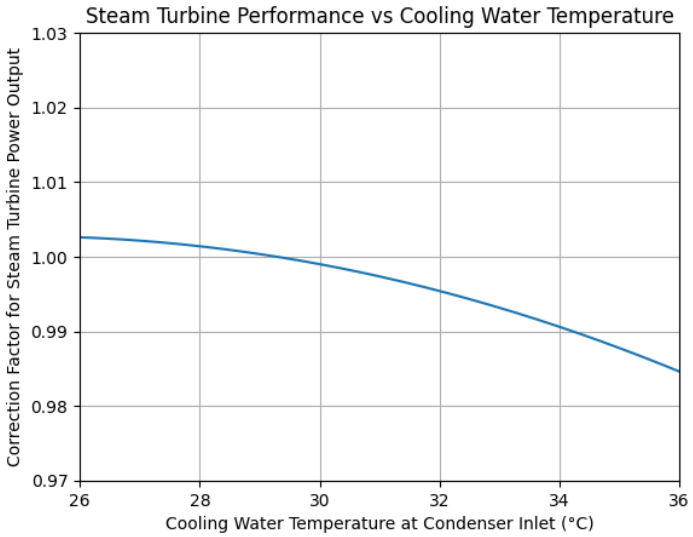

Figure 3. 9 SteamTurbine Performance Graph of Block 2 with Respect to Condenser Inlet Temperature

Based on the graph and the corresponding manual book, the regression equation used to determine the correction factor is expressed as follows:

$$y = 0{,}000000277764x^5 - 0{,}000040605804x^4 + 0{,}002358831477x^3 - 0{,}068281505144x^2 + 0{,}986499617454x - 4{,}688189497273$$

For the steam turbine unit, the effect of increasing seawater temperature was analyzed based on the relationship between steam turbine (ST) power output and circulating water temperature at the condenser inlet, expressed as a fifth-degree polynomial equation. To determine the sensitivity value, the equation was first differentiated to obtain the first derivative (dy/dx), representing the slope of the curve or the change in output for each 1°C increase in seawater temperature. The first derivative was then evaluated at specific temperatures: 30°C as the reference temperature, and 31.04°C and 30.81°C as the projected temperatures for 2030 and 2050, respectively. Using this approach, the calculated steam turbine output in 2030 at 31.04°C is 0.99845 of its rated capacity, equivalent to 69.89 MW. For 2050, at 30.81°C, the output is 0.99904 of capacity, equivalent to 69.93 MW. These results indicate power reductions of 0.261% in 2030 and 0.248% in 2050. The increasing absolute sensitivity value suggests that as condenser temperature rises, steam turbine performance becomes increasingly vulnerable to additional seawater temperature increases; each degree of warming in the future will result in a greater power reduction compared to present conditions.

3.4.3 Sensitivity to Sea Level Rise

The condition of the power plant area under projected sea level rise was assessed for the years 2030 and 2050. The sea level rise projections previously calculated (Table 3.1) were used as the basis for this analysis. Subsequently, the Copernicus GLO-30 Digital Elevation Model (DEM) and IPCC AR6 sea level rise (SLR) raster datasets were compiled. The study area was defined using a polygon obtained from Google Earth. The analysis was conducted for 2030 and 2050 under the SSP1-2.6, SSP2-4.5, and SSP5-8.5 scenarios. All SLR data were provided in raster format with units in millimeters and were converted to meters prior to analysis.

Intrusion sensitivity was evaluated within the polygon encompassing the Muara Karang Combined Cycle Power Plant area. Statistical results indicate that the average sensitivity value reaches 0.975 (on a 0–1 scale), which is categorized as very high sensitivity. Nearly all pixels within the area exhibit values of 1.0 or close to 1.0, indicating extreme vulnerability to seawater intrusion even under low SLR scenarios. The spatial plots for each scenario in 2030 and 2050 are presented below.

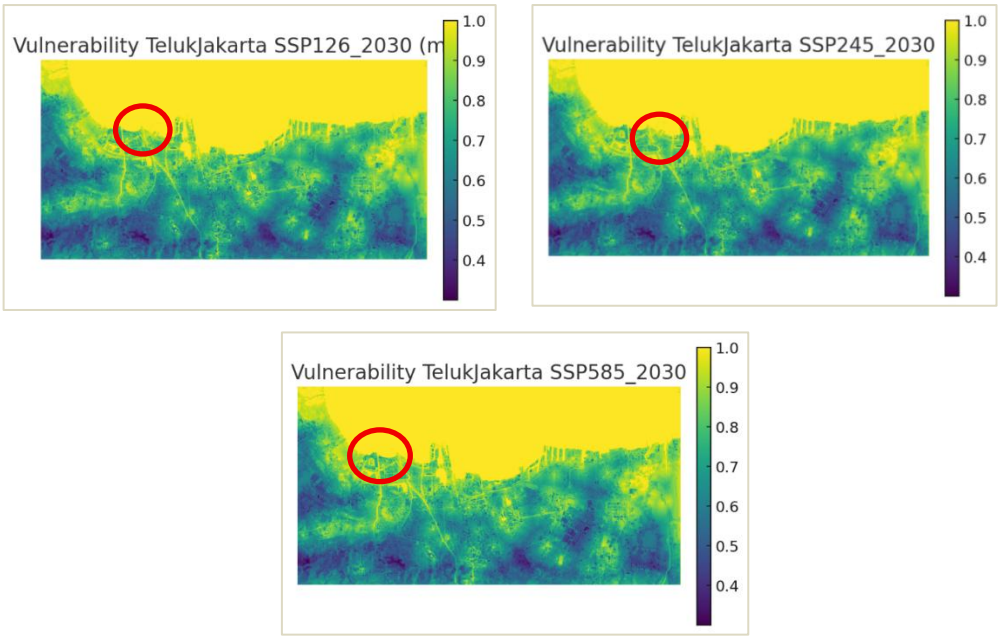

Figure 3. 10 Sea Level Rise Projection 2030

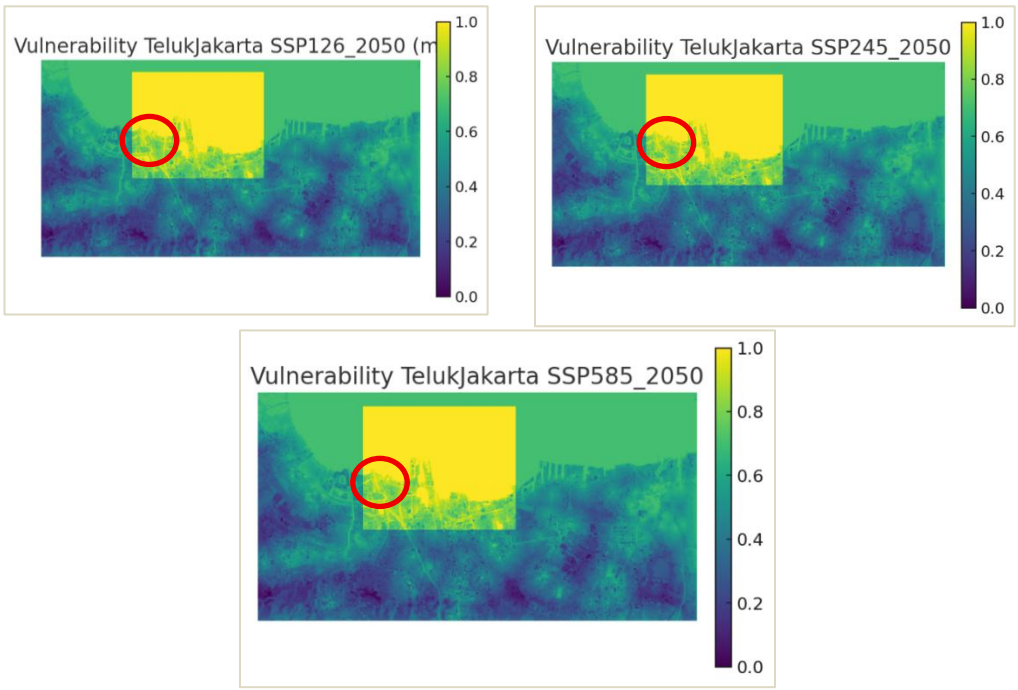

Figure 3. 11 Sea Level Rise Projection 2050

The 2050 map indicates both intensification and spatial expansion of vulnerability compared to 2030. Areas that were previously classified as low to moderate vulnerability in 2030 tend to shift toward moderate to high categories, while zones initially categorized as high are projected to escalate to very high vulnerability. Spatially, highly vulnerable areas expand along the coastline and extend inland into low-elevation zones, including areas surrounding critical energy and utility infrastructure.

3.4.4 Total Sensitivity

The calculation results of each sensitivity value are calculated in total to get 1 sensitivity value. The sensitivity value is calculated based on the weight of each sensitivity, namely sensitivity to ambient air temperature, sensitivity to sea surface temperature, and sensitivity to sea level rise. Vulnerability assessment approaches with composite indices almost always require indicator weighting. *Evidence-based weighting* replaces or complements this with weights derived from the data (e.g. PCA, entropy, random forest, correlation with impact) so that it is more objective. Conceptually, *evidence-based weighting* reduces subjectivity, increases validity and transparency, and is easier to maintain in the context of public policy (Li, *et al.*, 2022). The Sensitivity (S) component is prepared to represent the level of sensitivity of the Muara Karang PLTGU power plant system on the coast of Jakarta Bay to climate change and coastal dynamics. In this discussion, the sensitivity indicator is divided into 3 main indicators, namely:

C1 = sensitivity to increased ambient air temperature
C2 = sensitivity to rising sea surface temperature/cooling water temperature (SST)
C3 = sensitivity to seawater intrusion

To determine the weighting factors, a systematic literature extraction was conducted focusing on the impacts of ambient air temperature, cooling water temperature/SST, and seawater intrusion on coastal power plants. Each selected study was evaluated by the author using consistent criteria, a limited scoring scale, and subsequent weight normalization to ensure that the results were not influenced by individual subjective preferences. The assessment criteria were based on relevance, reliability, and consistency, using a scoring scale of 1–3. The evaluation results from 18 selected articles were averaged for each indicator, and the final weighting values are presented in the table below.

Table 3. 6 Sensitivity Weight Calculation

Indicator Code	Relevance	Reliability	Consistency	Total score	Final weight
C1	2,833	3,000	2,833	8,667	0,364
C2	2,333	3,000	3,000	8,334	0,350
C3	2,000	2,167	2,667	6,834	0,287
Total				**23,835**	**1.000**

After the final weight for sensitivity is known, sensitivity calculations can be carried out in the 2030 and 2050 projection years. Furthermore, the value is plotted in the category of sensitivity values to determine the sensitivity classification according to Table 3.7.

Table 3. 7 Sensitivity Value Category

Sensitivity Value Range	Category
0 – 0,2	Very Low
0,2 – 0,4	Low
0,4 – 0,6	Medium
0,6 – 0,8	High

0,8 – 1	Very High

The result of sensitivity calculation both in 2030 and 2050 are as follows:

Table 3. 8 Sensitivity Calculation 2030

Criteria	S (raw)	S_min	S_max	I (0-1)	Weight	Final score
C1	47.7553	43.8137	52.7087	0.4431	0.3640	0.1613
C2	0.2684	0.5418	0.2442	0.9184	0.3500	0.3215
C3	0.9500	0.9000	1.0000	0.5000	0.2870	0.1435
					S (Sensitivity) 2030	**0.6263**
					Category	**High**

Table 3. 9 Sensitivity Calculation 2050

Criteria	S (raw)	S_min	S_max	I (0-1)	Weight	Final score
C1	48.7290	43.8137	52.7087	0.5526	0.3640	0.2011
C2	0.2760	0.5418	0.2442	0.8932	0.3500	0.3126
C3	1.0000	0.9000	1.0000	1.0000	0.2870	0.2870
					S (Sensitivity) 2050	**0.8008**
					Category	**Very High**

3.5 Adaptive Capacity Analysis

Adaptive capacity represents the ability of a power generation system to anticipate, respond to, and minimize the adverse impacts of climate change or extreme events, such as tidal flooding, intense rainfall, and sea level rise. The higher the adaptive capacity of a power plant, the greater its ability to maintain operational performance and prevent significant disruptions to the energy production system.(Alam et al., 2017; Kiesel et al., 2022; Ray et al., 2020; Zhang et al., 2021).

Based on the assessment results, the following score was obtained; however, continuous improvements are necessary to maintain the relevance and readiness of the adaptive system in the future.

Table 3. 10 Adaptive Capacity Score

Components	Score	Weight (%)	Weighted Value
Upgrading Technology and Efficiency of Generating Units	5	20	1
Protective Embankment	5	20	1
Flood Pump	5	20	1
SOP & Emergency Response Team	5	20	1
Infrastructure Maintenance	4	20	0.8
Total		**100**	**4,8/ 5.00**

From the results of the values obtained, it is necessary to normalize on a scale of 0-1. Normalization is calculated by dividing the score by the maximum value, so that the following values are obtained

$$AC_{norm} = \frac{Adaptive\ Capacity\ score}{Maximum\ score} = \frac{4{,}8}{5{,}00} = 0{,}96$$

Thus, the indicators of the adaptive capacity of PLTGU can be categorized in the "high" level, as they already have comprehensive structural and non-structural mechanisms to deal with potential disruptions due to climate change. However, periodic improvements to the design of the embankment and pump system, as well as evaluation of the effectiveness of SOPs based on actual events, still need to be carried out to maintain the relevance and readiness of the adaptive system in the future.

3.6 Vulnerability Assessment

The discussion of technical aspects in this section discusses the factors that affect the vulnerability of the power plant. Vulnerability will be measured through 3 points, namely, *Exposure*, *Sensitivity*, and *Adaptive Capacity.* In choosing an indicator, it is necessary to know the purpose of vulnerability assessment, scale, level method adopted, availability and access to data (Sharma *et al.*, 2018). The indicators calculated in this discussion are exposure, among others, ambient air temperature, seawater temperature, sea level rise. The Sensitivity Indicator is seen from the data on the efficiency of the plant and the condition of the infrastructure. The Adaptive Capacity Indicator is seen from the availability of protective infrastructure and institutional completeness that already exists.

The Vulnerability Index (VI) is calculated as the average of the three main components, namely Exposure (E), Sensitivity (S), and adaptive capacity (AC), which refers to Equation 2.12, in the condition that all values have been normalized, The values obtained from the next calculation can be categorized referring to the following classifications:

Table 3. 11 Classification of Vulnerability Value Categories

Value Range	Category
0 – 0,2	Very Low
0,2 – 0,4	Low
0,4 – 0,6	Medium
0,6 – 0,8	High
0,8 – 1	Very High

Vulnerability calculation result in 2030 and 2050 are as follows:

Table 3. 12 Vulnerability Calculation in 2030 and 2050

Year	And	S	AC	VI	Category
2030	0,42	0,629	0,96	0,36	Low
2050	0,51	0,799	0,96	0,45	Medium

CONCLUSION

The exposure assessment results for 2030 and 2050 indicate that climate-related exposure falls within the “Moderate” category. Meanwhile, the sensitivity values are classified as “High” and “Very High,” respectively. However, the adaptive capacity

assessment remains within the "High" category. Consequently, the overall climate vulnerability assessment, based on ambient temperature, sea surface temperature, and sea level rise components, for the Muara Karang Power Generation Unit yields values of 0.36 in 2030 and 0.45 in 2050, corresponding to "Low" and "Moderate" vulnerability categories, respectively. This study considers only the partial reduction in power output from gas turbines and steam turbines, rather than the entire PLTGU cycle. The use of alternative datasets or correction methods may be applied in future research to compare and validate the results of this study.

REFERENCES

Alam, M., Alam, K., & Mushtaq, S. (2017). Climate change adaptation and resilience in energy systems. *Renewable and Sustainable Energy Reviews*, *75*, 654–663.

Ashrafi, H., & Parhizkar, T. (2023). Electricity sector resilience in response to extreme weather and climate-related events: Tools and datasets. *The Electricity Journal*, *36*(6), 107290.

Badan Pusat Statistik. (2024). *Jakarta Utara dalam angka 2024*. Badan Pusat Statistik.

Beyer, R., Krapp, M., & Manica, A. (2020). An empirical evaluation of bias correction methods for palaeoclimate simulations. *Climate of The Past*, 16, 1493-1508. https://doi.org/10.5194/cp-16-1493-2020.

Bompard, E., Napoli, R., & Xue, F. (2023). Power grid resilience enhancement under climate-related extreme events. *Electric Power Systems Research*, *219*, 109254.

Burillo, D., Chester, M. V, Pincetl, S., & Fournier, E. (2019). Climate change impacts on electricity demand in California. *Climatic Change*, *152*(3), 495–509.

Carleton, T., & Hsiang, S. (2016). Social and economic impacts of climate on energy demand. *Science*, *353*(6301), aad9837.

Craig, M. T., Cohen, S., & Macknick, J. (2018). Water constraints and electricity generation in a changing climate. *Nature Energy*, *3*(6), 474–480.

Firman, T., Surbakti, I. M., Idroes, I. C., & Simarmata, H. A. (2011). Potential climate-change related vulnerabilities in Jakarta: Challenges and current status. *Habitat International*, *35*(2), 372–378. https://doi.org/10.1016/j.habitatint.2010.11.011

Handayani, K., Filatova, T., & Krozer, Y. (2019). The vulnerability of the power sector to climate variability and change: Evidence from Indonesia. *Energies*, *12*(19), 3640.

Intergovernmental Panel on Climate Change. (2021). Climate Change 2021: The Physical Science Basis. Contribution of Working Group I to the Sixth Assessment Report of the Intergovernmental Panel on Climate Change. Cambridge University Press. https://doi.org/10.1017/9781009157896

Jia, Y., Xiao, K., Lin, M., & Zhang, X. (2022). Analysis of Global Sea Level Change Based on Multi-Source Data. *Remote. Sens*., 14, 4854. https://doi.org/10.3390/rs14194854.

Jin, S., Wei, Z., Wang, D., & Xu, T. (2023). Simulated and projected SST of Asian marginal seas based on CMIP6 models. *Frontiers in Marine Science*, 10, 1178974. https://doi.org/10.3389/fmars.2023.1178974.

Li, F., Yigitcanlar, T., Nepal, M., Thanh, K., & Dur, F. (2022). Understanding Urban Heat Vulnerability Assessment Methods: A PRISMA Review. *Energies*, *15*(19), 6998. https://doi.org/10.3390/en15196998.

Kiesel, K., Dilley, M., & Young, J. (2022). Resilience of urban electricity systems under extreme weather conditions. *Energy Research & Social Science*, *88*, 102514.

Martin, M., Ghent, D., Pires, A., Göttsche, F., Cermak, J., & Remedios, J. (2019). Comprehensive In Situ Validation of Five Satellite Land Surface Temperature Data Sets over Multiple Stations and Years. *Remote. Sens*., 11, 479.

https://doi.org/10.3390/rs11050479.
Mukherjee, S., & Nateghi, R. (2017). Climate sensitivity of end-use electricity consumption in the built environment. *Applied Energy*, *185*, 943–955.
NOAA (2024). Climate Change: Ocean Heat Content and Sea Surface Temperature. National Oceanic and Atmospheric Administration. Retrieved from https://www.climate.gov/news-features/understanding-climate/climate-change-ocean-heat-content
Pan, F., Wu, X., Zeng, Q., Tang, R., Wang, J., Lin, X., You, D., Wen, J., & Xiao, Q. (2024). A coarse pixel-scale ground "truth" dataset based on global in situ site measurements to support validation and bias correction of satellite surface albedo products. *Earth System Science Data, 16*(1), 161-176. https://doi.org/10.5194/essd-16-161-2024.
Panteli, M., & Mancarella, P. (2015). The grid: Stronger, bigger, smarter? Presenting a conceptual framework of power system resilience. *IEEE Power and Energy Magazine*, *13*(3), 58–66.
Panteli, M., Trakas, D. N., Mancarella, P., & Hatziargyriou, N. D. (2017). Power systems resilience assessment: Hardening and smart operational enhancement strategies. *Proceedings of the IEEE*, *105*(7), 1202–1213.
Petrakopoulou, F., Robinson, A., & Olmeda-Delgado, M. (2020). Impact of climate change on fossil fuel power-plant efficiency and water use. *Journal of Cleaner Production*, 273, 122816. https://doi.org/10.1016/j.jclepro.2020.122816.
Ray, P., Wenz, L., & Levermann, A. (2020). Future global energy demand and the role of climate variability. *Environmental Research Letters*, *15*(12), 124053.
Roxy, M. K., et al. (2020). Pacific Ocean Warming and its Impact on Tropical Climate Variability. *Nature Reviews Earth & Environment,* 1(8), 517–532. https://doi.org/10.1038/s43017-020-0073-0
Salehie, O., Jamal, M., Ismail, Z., Othman, I., Ishak, D., & Shahid, S. (2024). Projected Changes in Southeast Asian Sea Surface Characteristics Using CMIP6 GCMs. *Earth Systems and Environment*, 1-19. https://doi.org/10.1007/s41748-024-00480-3.
Scafetta, N. (2023). Impacts and risks of "realistic" global warming projections for the 21st-century. *Geoscience Frontiers*, *15*(2), 101774. https://doi.org/10.1016/j.gsf.2023.101774.
Stanton, M. C. B., Dessai, S., & Paavola, J. (2016). A systematic review of the impacts of climate variability and change on electricity systems in Europe. *Energy*, *109*, 1148–1159.
Sung, H., Kim, J., Lee, J., Shim, S., Boo, K., Ha, J., & Kim, Y. (2021). Future Changes in the Global and Regional Sea Level Rise and Sea Surface Temperature Based on CMIP6 Models. *Atmosphere*. https://doi.org/10.3390/atmos12010090
Surya, M. Y., He, Z., Xia, Y., & Li, L. (2019). Impacts of sea level rise and river discharge on the hydrodynamics characteristics of Jakarta Bay (Indonesia). *Water*, *11*(7), 1384. https://doi.org/10.3390/w11071384
Van Vliet, M. T., Wiberg, D., Leduc, S., & Riahi, K. (2016). Power-generation system vulnerability and adaptation to changes in climate and water resources. *Nature Climate Change*, *6*(4), 375–380.
Varrani, A., & Nones, M. (2018). Vulnerability, impacts and assessment of climate change on Jakarta and Venice. *International Journal of River Basin Management*, *16*(4), 439–447. https://doi.org/10.1080/15715124.2017.1387125
Zhang, Y., Wang, J., & Chen, Y. (2021). Assessing climate resilience of power infrastructure in coastal megacities. *Sustainable Cities and Society*, *68*, 102768.
Zhou, Y., Eom, J., & Clarke, L. (2019). Future changes in heating and cooling degree days and their impacts on electricity demand. *Energy Economics*, *84*, 104495.